Avoided crossings, scars, and transition to chaos

F. J. Arranz, F. Borondo, and R. M. Benito

Citation: The Journal of Chemical Physics **107**, 2395 (1997); doi: 10.1063/1.474582
View online: http://dx.doi.org/10.1063/1.474582
View Table of Contents: http://scitation.aip.org/content/aip/journal/jcp/107/7?ver=pdfcov
Published by the AIP Publishing

Avoided crossings, scars, and transition to chaos

F. J. Arranz and F. Borondo
Departamento de Química, C-IX, Universidad Autónoma de Madrid, Cantoblanco - 28049 Madrid, Spain

R. M. Benito
Departamento de Física y Mecánica, Escuela Técnica Superior de Ingenieros Agrónomos, Universidad Politécnica de Madrid, 28040 Madrid, Spain

(Received 3 March 1997; accepted 6 May 1997)

The correlation diagram of the LiNC/LiCN isomerizing system as a function of $\hbar$, taken as a parameter, is considered in conditions of widespread classical chaos. Two series of isolated avoided crossings of very different nature, involving states related by the same 1:8 quantum resonance condition, are characterized and the corresponding interaction matrix elements between adiabatic states analytically calculated and analyzed. One of these series has been found to separate two distinct regions: one for smaller values of $\hbar$ (at any given energy) corresponding to regular states, i.e., with a definite nodal pattern, and the other of much more stochastic behavior. Moreover, the effect of the interaction involved in these avoided crossings is to mix the regular wave functions giving rise to wave functions strongly scarred by the periodic orbits of the associated 1:8 classical resonance. This result constitutes an interpretation of the scarring effect from a new perspective. © *1997 American Institute of Physics.* [S0021-9606(97)01631-0]

I. INTRODUCTION

Avoided crossings (AC) in Born–Oppenheimer potential energy curves (or surfaces) are very important in the understanding of many dynamical processes, such as charge transfer, mutual neutralization, or predissociation.[1] As the corresponding states evolve as a function of a parameter, e.g., the internuclear distance in the case of atomic collisions, the potential curves may eventually get close, but due to the non-crossing rule of Wigner and von Neumann[2] they must avoid crossing (if they have the same symmetry). In such regions the terms neglected in the Born–Oppenheimer approximation become important, causing a potentially strong interaction between the curves. The region of interaction can be very localized in the parameter space, giving rise to a sharp AC, or correspond to a broader area, depending on the underlying physical non-adiabatic mechanism.[3] Many simple models, e.g., Landau–Zener, Demkov, Nikitin–Demkov,[1] have been described in the literature to cope with the different possibilities.

In the early eighties, Marcus and coworkers published a series of papers[4] in which they considered ACs in connection with the quantum manifestations of classical chaos[5] in systems of coupled anharmonic oscillators. They found the existence of ACs in the eigenvalues of the corresponding Hamiltonians as a parameter coupling the vibrations was varied.[4(a),4(b)] These states when quantized using a primitive semiclassical approximation cross[4(c)] instead of avoiding doing it. This indicates that the AC is due to classically forbidden trajectories and the splitting is obtained when quantized at a higher (Fourier transform[4(d)] or uniform[4(e)]) semiclassical level.[6] A similar calculation has been carried out recently by Joyeux.[7]

Moreover, these ACs when isolated were related to classical resonance conditions,[4(b)] the magnitude of the splitting being related to the width of the resonance zone. To this respect, Ozorio de Almeida[8] and Roberts and Jaffé[9] pointed out that the two states involved do not have to be located in the classical resonance zone. There is no contradiction between these two results, as shown by Heller,[10] since even in the second case the splitting is governed by the resonance condition. Heller, Stechel, and Davis[10,11] put the emphasis in the physical interpretation of the ACs and stressed their relation to ''dynamical tunneling'' and the intramolecular vibrational relaxation (IVR) associated to it. Contrary to usual tunneling, dynamical tunneling is not caused by barriers in the potential, but rather by constraints due to the approximate conservation of certain magnitudes, similar to the centrifugal barrier that appears in the familiar treatment of the motion under central forces.

Another possibility, which may happen depending on the characteristics of the system and the energy range considered, is that many ACs appear overlapping in a certain region of parameter values. In these situations the corresponding wave functions strongly mix, and this regime has been related[4(a),4(b)] to the existence of a mechanism for quantum stochasticity.[5,12]

The relation between ACs, tunneling, and chaos in time-dependent systems has also been considered in the literature.[13,14]

Avoided crossings as a criterion for ''quantum chaos'' have also been studied from other perspectives. In an early paper Pomphrey,[15] based on the conjecture due to Percival that irregular states should be very sensitive to small changes in the Hamiltonian,[16] suggested using eigenvalue second differences to ascertain the character of the different states: small values for regular states and large values for chaotic states. More recently, other authors[17] have examined the distribution of eigenvalue curvatures in classically chaotic systems.

In relation to the present discussion, a very interesting point was raised by both Marcus *et al.*[4(a)] and Heller,[10] which

is the dependence of the AC on the value of $\hbar$ and the density of states. Tunneling is known to vanish exponentially as $\hbar \to 0$. However, if the density of states is sufficiently high, as it is frequently the case in polyatomic molecules, even a small tunneling interaction may be enough to affect several vibrational states,[18] inducing for example profound changes in the corresponding molecular spectra. Pechukas[19] in 1983 made a first attempt to study level dynamics, considering the motion of energy spectra in the semiclassical limit ($\hbar \to 0$). This approach allows the use of some techniques used in statistical mechanics. Other authors[20] after him carried out similar studies considering the role of ACs.

In the case of systems with more than two degrees of freedom, the competing mechanism for IVR due to Arnold diffusion[21] must be taken into account, although very little is known about this process for realistic systems.[22]

In a previous Communication to this journal,[23] hereafter called paper I, we presented a preliminary study of the correlation diagram for the vibrational states of the LiNC/LiCN isomerizing system as a function of $\hbar$ (or equivalently the atomic masses) taken as a parameter. This molecule has been extensively studied in the past[23–27] in connection with the quantum manifestations of classical chaos. The Li–NC/Li–CN bending motion is very floppy and chaos sets in at relatively low energies. In paper I it was shown how a transition from irregularity to order takes place as $\hbar$ decreases. This transition manifests at a quantum level in the structure of the wave functions and spectra. The reason is that as $\hbar$ decreases more and more states can be accommodated in the regular region around the two stable linear LiNC and LiCN isomers. This effect was illustrated by considering the 24th and 25th (at $\hbar = 1$ a.u.) vibrational states, which are known to be strongly scarred, respectively, by an unstable and a stable 1:8 periodic orbits (PO), both corresponding to the same resonance.[25] These states present at $\hbar \approx 1$ a.u. a broad AC, but this interaction vanishes at smaller values of $\hbar$. As this happens, the corresponding wave functions unmix and correlate to regular states with the result that the scarring effect disappears.

The term scar[28] was introduced for the first time by Heller to refer to a localization effect of the quantum probability density in configuration space, which can be correlated to classical orbits. Although some single eigenfunctions show this effect in conditions of low density of states, scarring is more of a property of groups of eigenstates,[26,29,30] and also influences low resolution molecular spectra.[31,32] Takami, in his semiclassical study of ACs,[33] suggested that in fully chaotic systems ACs are originated from long periodic orbits winding around scars.

In the present article we extend our previous study of paper I. In the first place, we present a more complete correlation diagram of energy eigenvalues versus $\hbar$ in the range $0.01 \leqslant \hbar \leqslant 3$ a.u. and $E/\hbar \leqslant 4000$ cm^{-1}. We have studied the different kinds of ACs present, characterizing them quantitatively. For this purpose, we have analytically calculated and analyzed the interaction matrix elements $\langle \phi_m | \partial / \partial \hbar | \phi_n \rangle$ between different eigenfunctions.[34] In this way, a different series of similar ACs have been described. Finally, a discussion of the relation of ACs with scars has been made.

The organization of the paper is as follows. In the next section we describe the model system used in our study and the computational method used to calculate, both vibrational states and interaction matrix elements. In Sec. III the results are presented and discussed, and Sec. IV is devoted to summarizing our conclusions. Finally, we end in the Appendix by presenting the explicit expression of the interaction elements for the wave functions used.

II. SYSTEM AND CALCULATIONS

In this section we present the system that we have chosen to study, briefly introducing the model Hamiltonian for LiNC/LiCN used in our calculations. We also describe the procedure used to compute the energy levels and wave functions of our system, and the analytical method used for the calculation of the coupling matrix elements $\langle \phi_m | \partial / \partial \hbar | \phi_n \rangle$.

A. Model and calculations

In this paper we investigate a two degrees of freedom Hamiltonian model for the LiNC/LiCN isomerizing molecular system, in which the C–N bond distance is hold frozen at its anionic equilibrium value $r_e = 2.186$ a.u. This approximation is very well justified since the C–N bond frequency is very high, and the corresponding coordinate separates easily from the rest of the nuclear motions. With this assumption, the classical vibrational Hamiltonian (i.e., the total rotational angular momentum equals to zero) is given by

$$H = \frac{P_R^2}{2\mu_1} + \frac{1}{2}\left(\frac{1}{\mu_1 R^2} + \frac{1}{\mu_2 r_e^2} \right) P_\theta^2 + V(R, \theta), \tag{1}$$

where μ_1 and μ_2 are the Li–CN and C–N reduced masses, respectively, R is the distance from the center of mass of the CN fragment to the Li atom, r_e the fixed N–C distance, θ the angle between the corresponding vectors (measured from the Li–CN linear configuration), and P_R and P_θ are the corresponding conjugate momenta. The *ab initio* potential energy surface $V(R, \theta)$ has been taken from the literature[35] and is shown in Fig. 1 as a contour plot. It presents two stable isomers at the linear configurations Li–NC and Li–CN. The Li–NC isomer is the most stable one, and both are separated by a small energy barrier. The minimum energy path connecting these two isomers has also been plotted in the figure as a dotted line.

Classical trajectories have been calculated using a Gear algorithm for the numerical integration of the Hamilton equations of motion corresponding to Eq. (1). Some POs, relevant for the discussions of the present paper, have been obtained using the method of propagation of symmetry lines,[36] applied in this case to the Li–NC isomer configuration, i.e., $\theta = 180°$. The results are presented in Fig. 2, where the unstable and stable POs corresponding to the 1:8 resonance in the Li–NC well discussed in paper I are shown in panels (a) and (b), respectively. We also present an unstable 1:6 Li–NC PO which is also relevant for the quantum behavior (scars) of our system [panel (c)], and a stable rotor PO in which the Li atom orbits around the CN fragment [panel

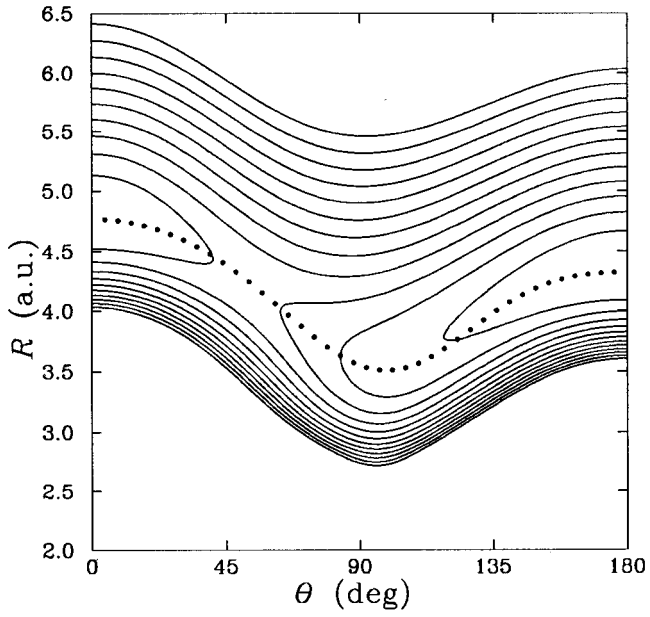

FIG. 1. Contour plot of the potential energy surface for the LiNC/LiCN isomerizing system. This surface has two minima corresponding, respectively, to the linear isomers LiNC and LiCN at the points $(R,\theta)=(4.3$ a.u.,180°) with energy 0, and (4.8 a.u., 0°) with energy 2281 cm^{-1}. These minima are separated by a saddle point located at (4.3 a.u.,48.4°) with energy 3455 cm^{-1}. The minimum energy path connecting the two wells is also plotted as a dotted line.

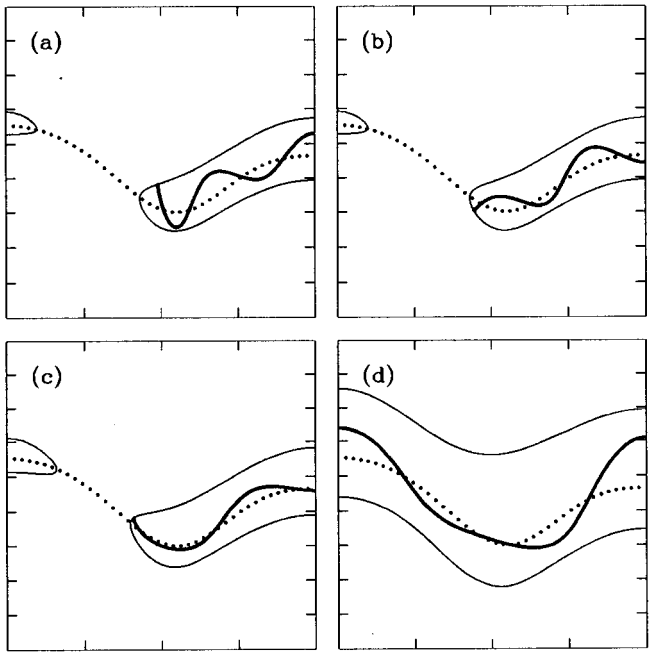

FIG. 2. Four periodic orbits relevant for the present paper (thick line) corresponding to resonances: (a) 1:8 unstable and (b) stable both at energy 2568 cm^{-1}; (c) 1:6 unstable at energy 2931 cm^{-1}; and (d) 1:8 stable (rotor) at energy 8052 cm^{-1}. The corresponding equipotential contour (thin line) and the minimum energy path (dotted line) has also been plotted in each panel. The axis used are the same as in Fig. 1.

(d)]. The first two orbits appear in a bifurcation of the principal family of POs, and the others have their origin in saddle-node bifurcations.[27]

The vibrational states corresponding to the Hamiltonian of Eq. (1) have been calculated using the discrete variable representation-distributed Gaussian basis (DVR-DGB) program of Bačić and Light.[37] Calculations were performed at different values of the physical constant $\hbar$ (actually scaling the atomic masses), taken as a parameter, thus obtaining a correlation diagram of energy levels. The calculation parameters appearing in the code of Bačić and Light were approximately optimized at each value of $\hbar$. For example, at $\hbar=1$ a.u. a basis set of 416 elements was used in the final diagonalization, obtaining 100 eigenvalues converged to within 0.1 cm^{-1}.

B. Interaction calculations

Similar to the results obtained by Marcus *et al.*,[4] and as we will see in the next section, our correlation diagram presents a series of ACs of different characteristics. The corresponding interactions are well described in terms of the associated coupling matrix elements corresponding to the variation with the correlation parameter, i.e., $\langle\phi_m|\partial/\partial\hbar|\phi_n\rangle$. This is analogous to the dynamical (radial or angular) couplings responsible for the non-adiabatic processes taking place in atomic collisions.[1,3,6] This type of couplings appears in the adiabatic representation of the Hamiltonian operator,

$$\hat{H}=\sum_n |\phi_n\rangle E_n\langle\phi_n|, \tag{2}$$

where $|\phi_n\rangle$ are the stationary states of $\hat{H}$, and E_n the corresponding eigenvalues. Alternatively, a diabatic representation[38] can be used, formed by states $|\chi_i\rangle$ which do not diagonalize $\hat{H}$ but preserve their character as the correlation parameter changes,

$$\hat{H}=\sum_i \sum_j |\chi_i\rangle\langle\chi_i|\hat{H}|\chi_j\rangle\langle\chi_j|. \tag{3}$$

In this representation the coupling matrix elements are null ($\langle\chi_i|\partial/\partial\hbar|\chi_j\rangle=0$), and the interaction comes from the Hamiltonian matrix elements $\langle\chi_i|\hat{H}|\chi_j\rangle$. Obviously, these two representations can be easily related. The adiabatic representation can be calculated by simply diagonalizing the diabatic one, and conversely diabatic states can be obtained as the result of making zero simultaneously all coupling matrix elements, which implies the integration of a system of coupled differential equations in the variable $\hbar$.[39]

In the case that the interaction is restricted to only two real states (isolated AC), the diabatic representation can be obtained from the adiabatic one using the following rotation matrix:

$$\begin{pmatrix}\langle\chi_1|\phi_1\rangle & \langle\chi_1|\phi_2\rangle\\ \langle\chi_2|\phi_1\rangle & \langle\chi_2|\phi_2\rangle\end{pmatrix}=\begin{pmatrix}\cos\xi & \sin\xi\\ -\sin\xi & \cos\xi\end{pmatrix}, \tag{4}$$

where the rotation angle ξ is obtained from the diabatic condition ($\langle\chi_i|\partial/\partial\hbar|\chi_j\rangle=0$, with $i,j=1,2$) expressed in the adiabatic basis set $\{|\phi_1\rangle,|\phi_2\rangle\}$, being the final result the differential equation,

$$\frac{d\xi}{d\hbar}=\left\langle \phi_1\left|\frac{\partial}{\partial\hbar}\right|\phi_2\right\rangle, \tag{5}$$

with the formal initial condition $\xi(\hbar=0)=0$. For the inverse transformation, i.e., for obtaining the adiabatic representation from the diabatic one, the angle ξ is given by

$$\xi(\hbar)=\frac{1}{2}\tan^{-1}\frac{2H_{12}}{H_{22}-H_{11}}, \tag{6}$$

where $H_{ij}=\langle\chi_i|\hat{H}|\chi_j\rangle$ are the diabatic Hamiltonian matrix elements. The relation $S(\hbar)=(H_{22}-H_{11})/2H_{12}$ between these matrix elements is known as the Stückelberg function, and its magnitude controls the interaction between the two corresponding adiabatic states.

Finally, we will mention that the coupling elements between the vibrational DVR-DGB eigenfunctions of LiNC/LiCN (see Sec. II A) have been analytically calculated using the Hellmann–Feynman theorem:[40]

$$\left\langle \phi_m\left|\frac{\partial}{\partial\hbar}\right|\phi_n\right\rangle=\frac{1}{E_n-E_m}\left\langle \phi_m\left|\frac{\partial\hat{H}}{\partial\hbar}\right|\phi_n\right\rangle. \tag{7}$$

The corresponding final expressions are given in the Appendix.

III. RESULTS AND DISCUSSION

The correlation diagram for the vibrational energy levels of LiNC/LiCN up to $E/\hbar=4000$ cm^{-1}/a.u. as a function of $\hbar$ is presented in Fig. 3. This includes, for example, the first 70 eigenvalues corresponding to $\hbar=1$ a.u. In our plot, we have chosen to represent in the vertical axis $E/\hbar$ instead of E to make the figure clearer. The reason for this is the following. At high energies the slope of the energy curves gets very high and some portions of the E vs $\hbar$ plot get too crowded, with the result that some curves get too close to allow for an adequate following of their evolution. However, this problem disappears in the type of representation used in Fig. 3, where, for example, the harmonic states located in the most stable Li–NC well would render horizontal lines, and those corresponding to the other isomer would appear as hyperbolas displaced vertically. As can be seen in the figure, some of our low lying states approach this behavior, at least for some range of values of the parameter $\hbar$.

The most interesting feature of Fig. 3 in relation to the goals of this paper is the existence of numerous ACs with very different physical characteristics. Some of them that will be discussed in this paper have been marked with open circles. As it is clearly appreciated, these ACs separate into two very distinct series. The first one, located on the left of the correlation diagram (circles in a thin line), corresponds to ACs for which the interaction region is extremely small, and confined to the immediate vicinity of the AC. The splittings due to the interactions can hardly be appreciated in the scale of the figure. The other series is located more to the right part

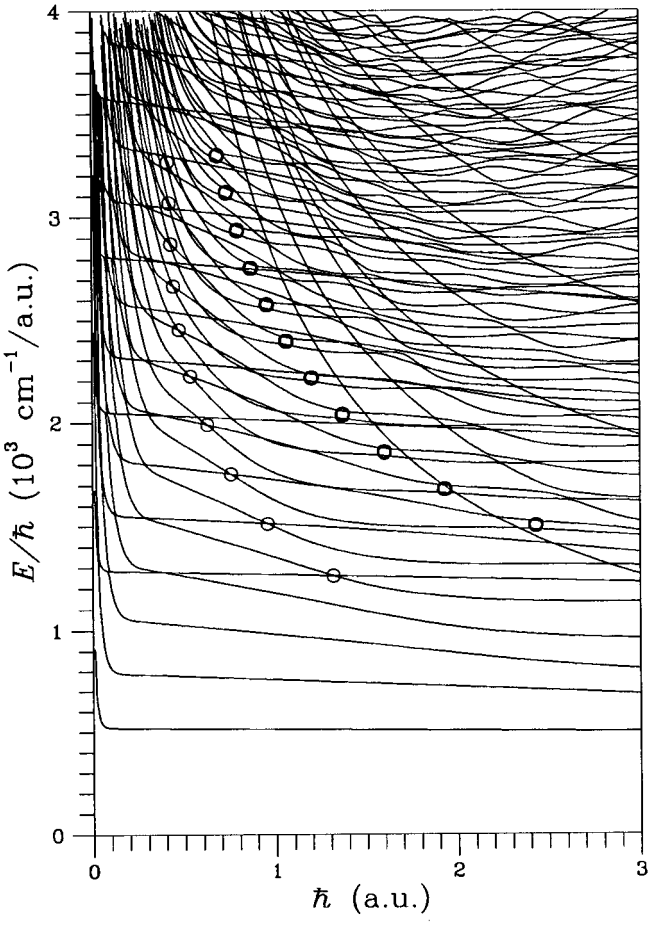

FIG. 3. The correlation diagram as a function of $\hbar$, taken as a parameter. Two series of avoided crossings have been marked with thin and thick open circles; they are referred to, respectively, as *left* and *right* series throughout the text.

of the correlation diagram, and the corresponding ACs have been marked with circles in a thick line. These ACs are much broader and present splittings of a much greater magnitude. Moreover, this second series of ACs seems to constitute the frontier or separation of two very different regions: one below it containing only isolated, sharp ACs, and another above it corresponding to a region of more intense interaction, crowded with many broad, overlapping ACs. According to Marcus' criterion for quantum stochasticity,[4] crossing this line would correspond to a transition from order to chaos and, as we will ascertain in this paper using more quantitative arguments, this is the case for the present system.

Actually, in paper I we examined this transition from order to chaos from the point of view of the scars of the corresponding wave functions and spectra in a particular case. In it, we discussed the interaction between states 24th and 25th, which is the first (in energy) broad AC that appears at $\hbar=1$ a.u. (see Fig. 3). Consideration of other values of $\hbar$ gave a clear picture of the evolution of the wave functions involved. Thus, at $\hbar=0.8$ a.u. the interaction is very small and the wave functions look very regular (see Fig. 2 of paper I), corresponding to states $(n_R,n_\theta)=(0,24)$ and $(1,16)$,

respectively.[41] As $\hbar$ increases, the two states begin to interact and mix in such a way that the resulting wave functions are strongly scarred by the unstable and stable POs, shown in Fig. 2, corresponding to the 1:8 resonance of the LiNC/LiCN system discussed in Ref. 25. This result indicates the prominent role of the classical 1:8 resonance, and is in agreement with the quantum number assignment of the unperturbed regular states (at $\hbar=0.8$ a.u.) made above, for which $|\Delta n_R|:|\Delta n_\theta|=1:8$.

In fact, when the complete correlation diagram is considered a whole series of these interactions appears (the right series of ACs in the correlation diagram in Fig. 3), each one at a different value of $\hbar$, which gets smaller as we progress up in the series. The states involved are the lowest to fulfill the 1:8 quantum resonance, since they correspond to quantum numbers $(0,8+2k)$ and $(1,2k)$, with $k\geqslant 0$ (in the figure only the ACs for $2\leqslant k\leqslant 12$ appear). The factor 2 multiplying the index k is due to the symmetry of the bending part of the LiNC/LiCN wave functions with respect to the linear configuration (see Ref. 41).

A similar situation occurs for the series of ACs on the left part of the correlation diagram, where the ACs corresponding to $k=0$ to 9 have been marked with thin circles. In this case, the ACs are much sharper and scars do not appear as a result of the ACs, although they correspond to states fulfilling the same 1:8 quantum condition. The reason for this is the following. As higher values of $\hbar$ are considered (going from the left to the right series of ACs) the LiNC/LiCN vibrational states need more ''phase space room'' and cannot accommodate themselves in the regular region around the Li–NC isomer (see Fig. 1 of paper I), extending into the chaotic sea. In the configuration space this corresponds to states very excited in the bending coordinate that has a significant part of their probability beyond the sharp curvature in the minimum energy path that occurs at $\theta=99°$. This is expected to originate a strong classical bobsled effect,[42] which mix the motions in the R and θ coordinates and originates chaos in this problem. These chaotic states present in general a complex nodal pattern and some of them appear scarred along POs. This can be investigated more quantitatively using the techniques described in Refs. 8,9, and this will be the subject of a future publication.

In order to study more deeply the interactions involved in the series of crossings that we have just described, let us consider now the coupling matrix elements. The corresponding results are shown in Figs. 4 and 5 for the left (L) and right (R) series, respectively, together with the transformation angles ξ derived from them (see Sec. II B). As it is seen in Fig. 3 all ACs take place at different values of the parameter $\hbar$, and then the corresponding couplings are centered at different points, $\hbar_{0k}^{\mathrm{L}}$ and $\hbar_{0k}^{\mathrm{R}}$, of the correlation diagram. In order to be able to present all the results in the same plot, the couplings have been shifted so that their maxima coincide at the new origin. The position $\hbar_{0k}^{\mathrm{L,R}}$ and value $M_k^{\mathrm{L,R}}$ of the coupling elements maxima, together with the asymptotic value of ξ, for the different ACs marked in Fig. 3 are presented in Table I. These values can be used to identify the different curves in Figs. 4 and 5. Note that as we progress in

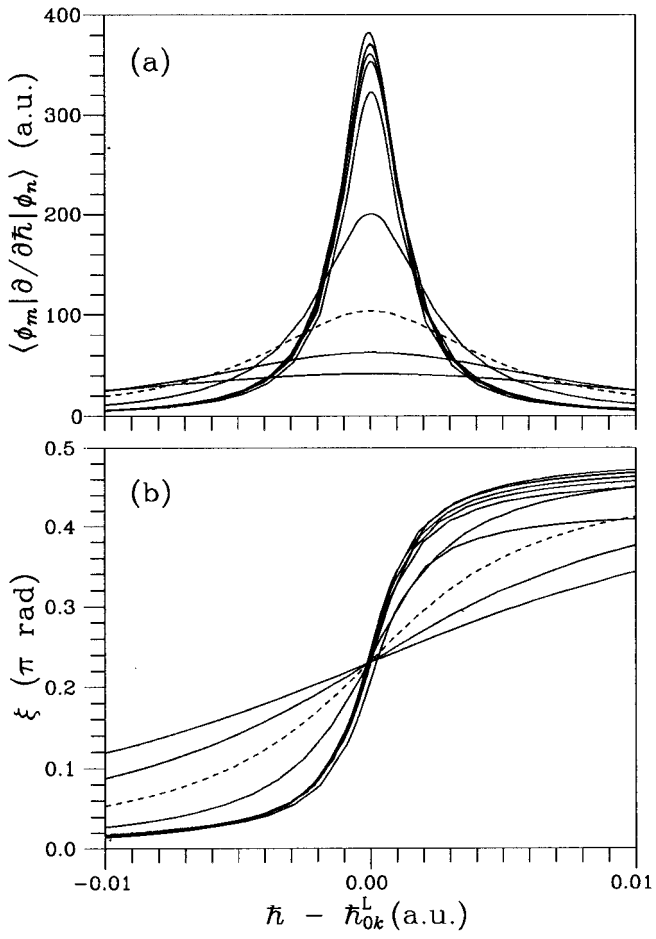

FIG. 4. (a) Coupling matrix elements $\langle\phi_n|\partial/\partial\hbar|\phi_m\rangle$ and (b) transformation angles ξ for the avoided crossings ($k=0$–9) in the left series of Fig. 3. The results have been shifted so that the maxima of the couplings (located at $\hbar_{0k}^{\mathrm{L}}$) coincide. The different curves can be identified by comparison with the results presented in Table I. The curves for $k=7$, which are discussed in detail in the text, have been represented in a dashed line.

the left series the coupling elements become slightly sharper and bigger from $k=0$ to 4, and abruptly decrease and become broader afterwards. In the right series the peaks monotonically increase getting at the same time sharper, except for the last one ($k=12$). The curves in panel (b) can be identified by taking into account that $\xi(\hbar)$ corresponds to the area enclosed below the coupling [see Eq. (5)], or by comparing their asymptotic values with the numerical values given in Table I.

Several comments concerning these figures are in order. In the first place, notice the difference (nearly two orders of magnitude) in the scales used in both figures. This is an indication that the interaction corresponding to the left ACs is only important in a much narrower range. In the second place, when examined, the couplings of both series look very similar since they all present a Lorentzian-type shape. However, when properly analyzed strong differences are revealed, which reflect the different underlying interactions. These differences are more clearly seen when considering the transformation angle ξ. The left ACs present sharper

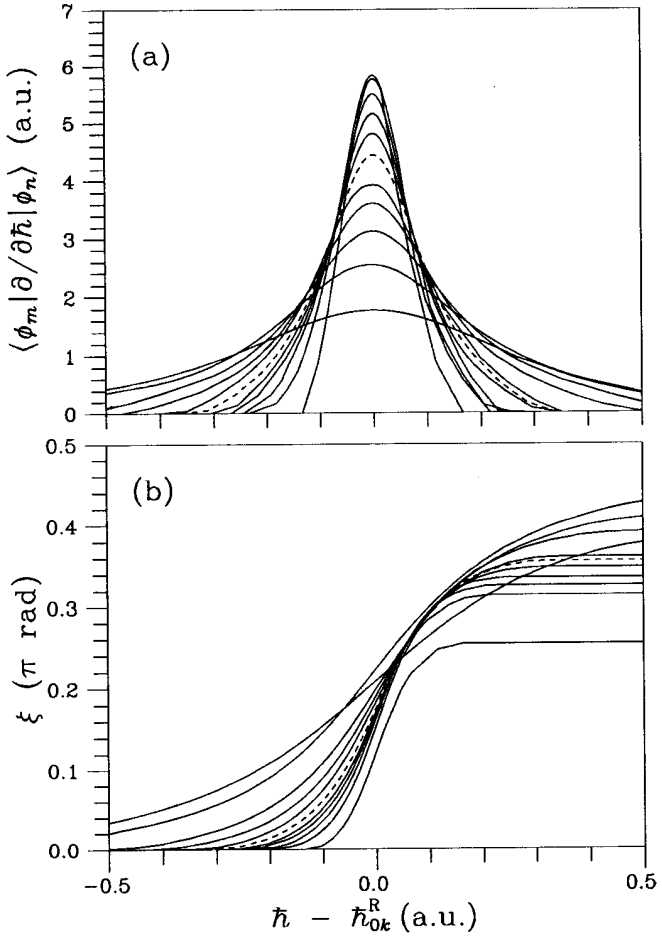

FIG. 5. The same as Fig. 4 but for the right series of avoided crossings with $k=2-12$.

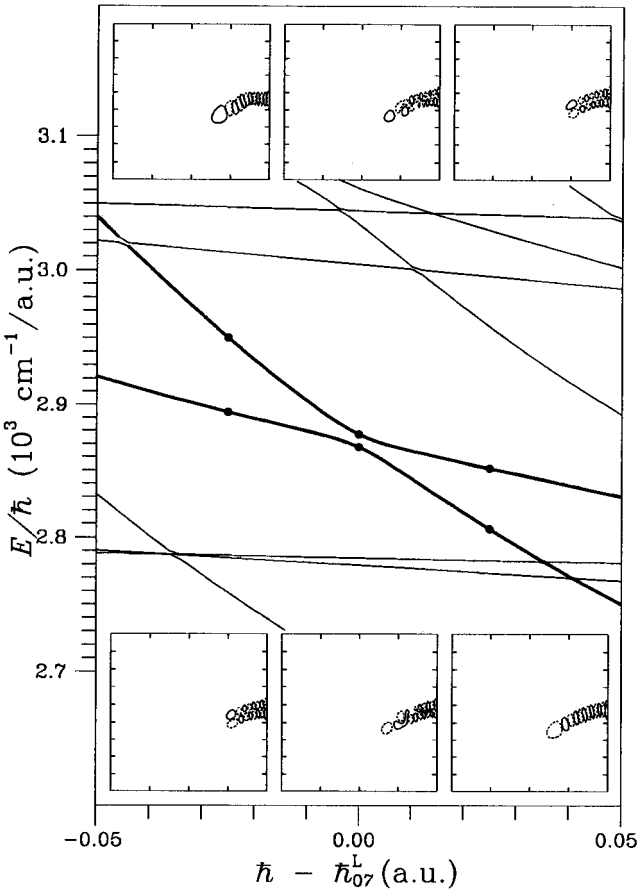

FIG. 6. Detail of the correlation diagram in the region of the $k=7$ left avoided crossing. The involved adiabatic energy curves are represented in a thick line and the wave functions corresponding to the points marked with dots are shown in the insets. Two contours corresponding to $\pm 10\%$ of the maximum value of the wave function has been represented in solid and dashed lines, respectively. The axes used are the same as in Fig. 1.

peaks than those on the series of the right; moreover, the former correspond to transformation angles that go from 0 to approximately $\pi/2$, while the others end at smaller values of ξ (0.25π - 0.40π) (see Table I). This difference in the asymptotic value of the transformation angle is very important since it implies that in the first case the involved adiabatic states undergo an exchange of character in the AC, while in the second the states get mixed after the AC. This effect is clearly illustrated in the next figures.

TABLE I. Position $\hbar^{L,R}_{0k}$ and value $M^{L,R}_k$ of the coupling elements maxima and asymptotic value of the transformation angles $\xi^{L,R}_k$ for the two series of avoided crossings (AC) marked in the correlation diagram of Fig. 3.

	Left series of ACs			Right series of ACs		
k	$\hbar^{L}_{0k}$ (a.u.)	M^{L}_k (a.u.)	$\xi^{L}_k(\infty)$ (π rad)	$\hbar^{R}_{0k}$ (a.u.)	M^{R}_k (a.u.)	$\xi^{R}_k(\infty)$ (π rad)
0	1.317	322.96	0.426	-	-	-
1	0.956	353.92	0.469	-	-	-
2	0.756	361.80	0.474	2.43	1.77	0.395
3	0.627	370.87	0.480	1.93	2.55	0.443
4	0.536	382.53	0.485	1.60	3.12	0.411
5	0.474	371.48	0.489	1.37	3.61	0.392
6	0.445	200.58	0.482	1.20	3.92	0.361
7	0.431	103.62	0.470	1.06	4.43	0.356
8	0.422	62.656	0.464	0.96	4.80	0.349
9	0.414	41.922	0.450	0.87	5.15	0.335
10	-	-	-	0.79	5.50	0.326
11	-	-	-	0.73	5.82	0.314
12	-	-	-	0.68	5.76	0.254

The portion of the correlation diagram corresponding to the left AC with $k=7$, together with the evolution across the AC of the two wave functions involved is presented in Fig. 6. Notice that the adiabatic (thick) curves have been smoothed by a partial diabatization procedure, done by simple continuation, in order to eliminate unwanted ACs with other curves (shown as a thin line in the figure), which are not relevant to the discussion presented here. To help in the discussion the corresponding coupling matrix element and transformation angle were identified in Fig. 4 by using a dashed line. The two relevant energy curves, which have been highlighted with a thick line in the figure, have different slopes, and they maintain their characters until they come to cross. At this point, and due to the Wigner–von Neumann non-crossing rule,[2] they have to avoid crossing. This process takes place through a complete exchange of the wave func-

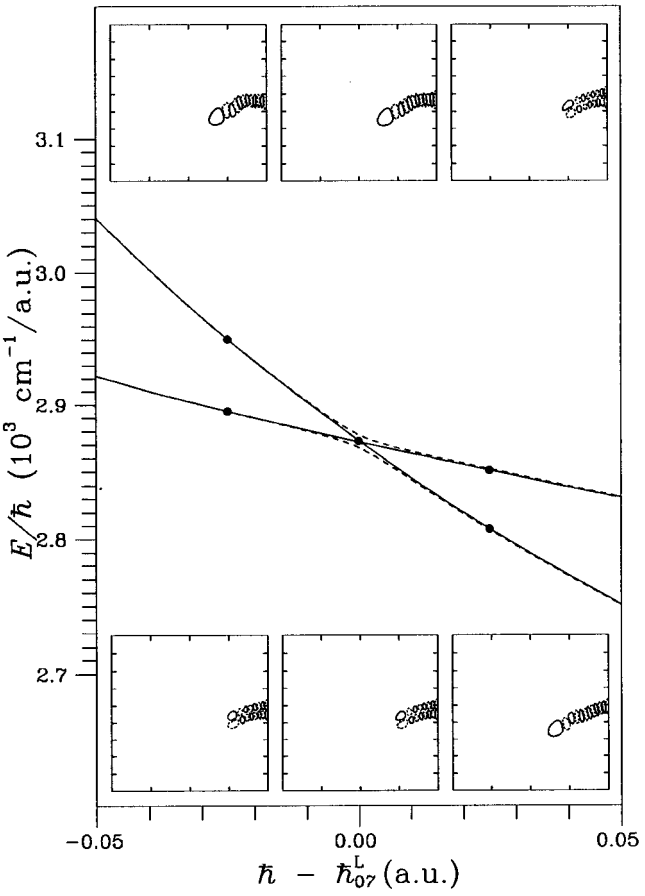

FIG. 7. Diabatic energy curves (full line) and wave functions (insets) at selected values of $\hbar$ corresponding to the avoided crossing presented in Fig. 6. The adiabatic energy curves have also been included in a dashed line to help interpret the figure. Two contours corresponding to $\pm 10\%$ of the maximum value of the wave function has been represented in solid and dashed line, respectively. The axis used are the same as in Fig. 1.

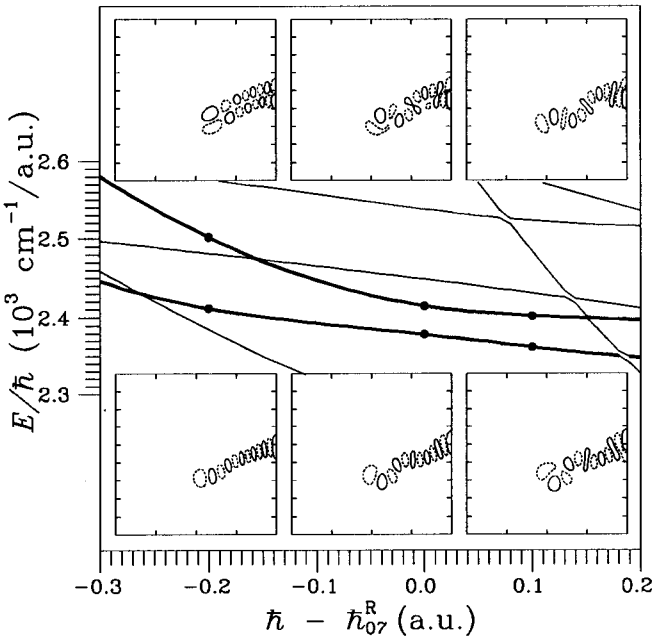

FIG. 8. The same as Fig. 6 but for the corresponding $k=7$ avoided crossing of the right series.

tions, which only mix in a very narrow range of $\hbar$ values around the AC, as can be seen in the insets to the figure. Consequently, the corresponding (character conserving) diabatic curves, which are presented in Fig. 7, cross each other at the AC, coinciding with the energy curves of the adiabatic states (plotted with a dashed line) immediately after and before the crossing. These diabatic states and curves have been calculated by integrating the corresponding coupling element, as described in Sec. II B. Totally similar results are obtained when other members of this series of ACs are considered.

Let us consider now the equivalent AC in the series on the right. The adiabatic curves and wave functions corresponding to $k=7$ are shown in Fig. 8. Again, the relevant adiabatic curves were highlighted with a thick line, and the corresponding coupling matrix element and transformation angle identified with dashed lines in Fig. 5. In this case, the AC takes place over a broader range of $\hbar$ values than in the previous case (remember the difference existing in the scales of both axis), consistent with the shape of the corresponding calculated coupling (see Fig. 5). More interesting is to consider the evolution with $\hbar$ of the involved wave functions, which can be followed in the insets to the figure. As can be seen in Fig. 8 (see also Fig. 5) for $\hbar-\hbar^{R}_{07}=-0.2$ a.u. the two adiabatic wave functions are practically decoupled, presenting very regular structures with a clear nodal pattern, which corresponds to states (0,22) and (1,14), respectively. As $\hbar$ increases, the two energy curves begin to approach and the wave functions start to interact noticeably. At this point the scar due to the POs of the classical 1:8 resonance discussed in Sec. II A becomes apparent. This scarring effect can be considered to be fully developed at $\hbar-\hbar^{R}_{07}\approx 0.1$ a.u., value which is well to the right of the maximum of the coupling (see Fig. 5), and the transformation angle is close to its asymptotic value. For $\hbar-\hbar^{R}_{07}\gtrsim 0.2$ a.u. the interaction that we are considering start to involve simultaneously other states, and the corresponding wave functions become either irregular or scarred by other POs different from those considered so far. Finally, as $\hbar$ gets even bigger there is a point in which the states become isomerizing, being delocalized among the two isomer wells of the system.

The corresponding diabatic curves and wave functions are presented in Fig. 9. It can be observed that in this case the curve crossing takes place at a positive value of $\hbar-\hbar^{R}_{07}$, i.e., for values of $\hbar$ bigger than that corresponding to the maximum of the coupling element, due to the different type of interaction involved. The insets show the evolution of the diabatic wave functions, which maintain a clearly defined nodal pattern corresponding to the regular structures $(n_R,n_\theta)=(0,22)$ and (1,14), respectively.

Let us consider now, in a systematic comparative way, the evolution of the pairs of wave functions involved in different ACs of the series appearing on the right of the corre-

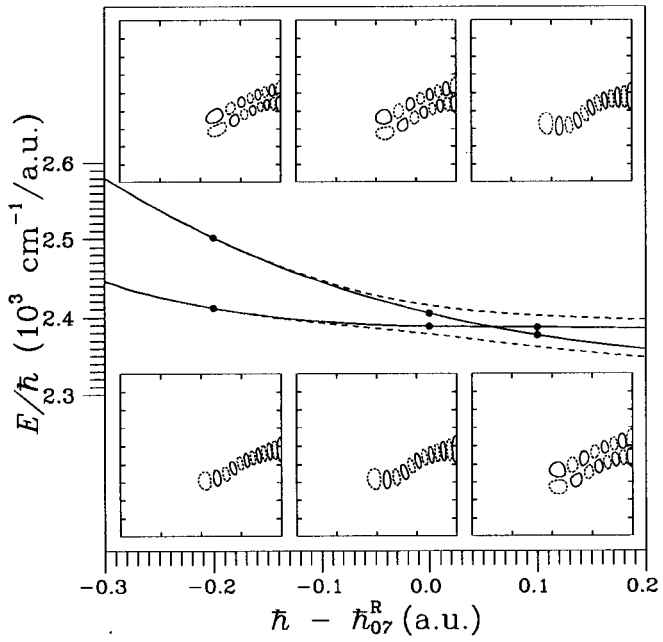

FIG. 9. The same as Fig. 7 but for the avoided crossing presented in Fig. 8.

lation diagram. The results are shown in Fig. 10, which requires some explanation. Each row in the figure corresponds to a different AC and has been labelled with the associated index k. In each one of them the two interacting wave functions, labelled at the top with their state number N (the integer, starting at $N=1$, indicating the order of the state in the energy scale), are shown at representative values of the parameter $\hbar$, also written on the top of each panel. These values of $\hbar$ have been chosen in the following way. The first two columns correspond to a point before the AC, where the involved coupling element is very small and there is a negligible interaction between the states. The wave functions are clearly regular and quantum numbers can be easily assigned. The difference among rows is that the involved states have an increasing degree of excitation in the bending mode along the minimum energy path as k increases. The corresponding number of bending nodes increases by two, starting from $(n_R,n_\theta)=(0,18)$ and $(1,10)$ for $k=5$ and going up to $(0,32)$ and $(1,24)$ for $k=12$. For all rows the 1:8 quantum resonance condition is fulfilled.

The next two columns correspond to values of $\hbar$ for which the interaction is fully developed, that is the involved coupling element has reached its maximum and decreased again. The corresponding wave functions, which are a continuation of the pair in the preceding columns, do not look regular any longer, but present a strong scar from the stable and unstable POs of the 1:8 resonance (see Fig. 1). Moreover, the number of nodes along the POs coincides with the number of nodes of the corresponding regular state $(0,8+2k)$. Notice that the state numbers at the top of the panels do not necessarily coincide with those on the first two columns since for intermediate values of $\hbar$ there may have been taken place sharp ACs, irrelevant for the present discussion as we explained above, which may have changed the state number.

Finally, in the last two columns points of $\hbar$ in the high value region have been selected. As it was said before, in this region the interaction gets more complicated and the wave functions are either irregular or scarred by other POs. For example, all wave functions presented in the fifth column are scarred by the 1:6 PO plotted in Fig. 2(c). A close examination of the avoided crossings reveals that in this case the scattering effect appears as the result of the simultaneous interaction of more than two states, which are already mixed by the 1:8 resonance. As a consequence the scarring effect of the 1:6 resonance cannot be explained in terms of regular states so simply as in the case discussed previously. Actually, the states in this column constitute a consecutive series of states excited along this PO, starting in the figure with a corresponding quantum number of 18 and ending at 32. Notice also that all wave functions in the series extend to approximately the same value of θ. This is easily understood if one considers that although the wave functions correspond to different values of the energy and quantum numbers (number of nodes) they come scaled by a different value of $\hbar$. This is also true for the previous series of wave functions. Similarly, the wave functions on the sixth column are all delocalized over the whole range of θ values, and correspond to isomerizing states for the LiNC⇌LiCN reaction. When examined carefully, they appear formed by two different functions joining at the region of the saddle: one located in the Li–NC well scarred by a PO, and the other corresponding to a regular state in the Li–CN well. Let us remark that this effect is not due to tunneling since all states presented there are well above the isomerization barrier. Also, this kind of state, which can be called *hybrid*, should not be mistaken with rotor states,[24] which present probability densities accumulated along single rotor POs and a different energy dependence on $\hbar$. Let us examine this argument in more detail in the next paragraph.

In Fig. 11 another portion of the correlation diagram of the LiNC/LiCN system at higher energies is shown. In it, one observes that some pieces of different energy curves (highlighted in a thick line) lie on straight lines presenting positive slopes. The corresponding diabatic behavior follows, in this case, the characteristic energy dependence of the rigid rotor model $E_J=\hbar^2J(J+1)/2I$. This assumption can be further confirmed by examination of the associated wave functions. Some of them, corresponding to selected values of $\hbar$ (marked with dots) along the diabatic curves are presented in the right part of the figure. It is seen that they all correspond to true rotor states, where the Li nucleus orbits around the CN fragment, with an increasing degree of excitation in the angular coordinate. The lowest wave function plotted presents 25 nodes in the range 0-π, value which is increased by one as we progress to higher diabatic curves. Moreover, it can be noticed that the probability density is well localized on the corresponding rotor PO shown in Fig. 2(d), contrary to what happens to the hybrid states on the last column in Fig. 10.

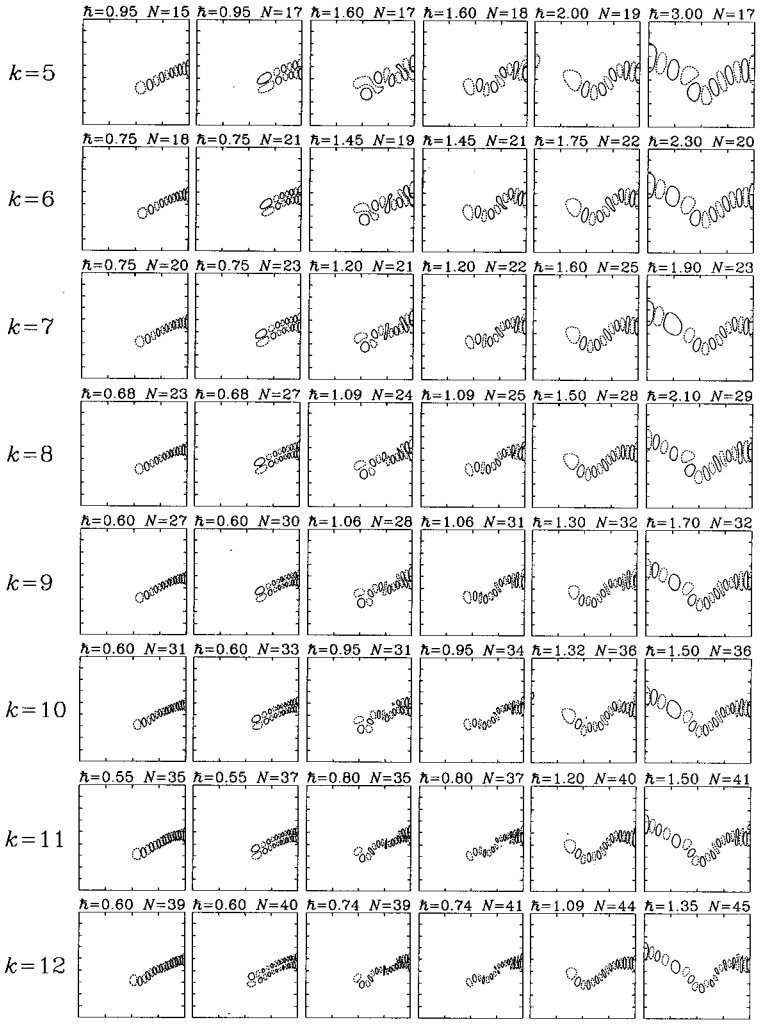

FIG. 10. Selected wave functions involved in different avoided crossings of Fig. 3 at selected values of $\hbar$. The number N, indicating the order of the state in the energy scale, is also indicated. Two contours corresponding to $\pm 10\%$ of the maximum value of the wave function has been represented in solid and dashed lines, respectively. The axes used are the same as in Fig. 1.

IV. SUMMARY AND CONCLUSIONS

The LiNC/LiCN system constitutes an ideal example for the study of chaos in molecular dynamics. It is described by a realistic potential energy surface, which includes many interesting features: anharmonicities, nonlinear couplings between modes, the possibility of isomerization, etc. The bending mode is very floppy and chaos sets in at modest excitation vibrational energies.

In the present paper, which is an extension of a previous Communication to this journal,[23] the correlation diagram of the LiNC/LiCN system as a function of $\hbar$, taken as a parameter, has been calculated and studied in detail. Two series of ACs of very different nature have been described, and the corresponding interaction matrix elements between the involved adiabatic states $\langle \phi_m | \partial / \partial \hbar | \phi_n \rangle$ analytically calculated using the Hellman–Feynman theorem. These couplings and their integrals ξ completely characterize the ACs.

For the ACs in the series taking place on the left of the correlation diagram the functions ξ tend asymptotically to $\pi/2$, which means that in the corresponding AC the interaction merely exchange the characters of two involved wave functions. All involved states present very regular wave functions, which for each AC, labelled by the index k, correspond to $(n_R, n_\theta) = (0, 8+2k)$ and $(1, 2k)$, so that a 1:8 quantum resonance condition is fulfilled.

On the other hand, for the right series of ACs the interaction between states, which are also related by the same 1:8 quantum condition, correspond to values of ξ sensibly smaller. This implies that in the AC the involved states get mixed, resulting in final wave functions which are strongly scarred by the two classical POs (stable and unstable) corresponding to a 1:8 classical resonance of the system. This constitutes, in our opinion, the main result of our work.

It should also be noticed that the different ACs of a series take place at different values of $\hbar$, so that the complete series of scarred states is not observable in a single quantum calculation, i.e., carried out at a fixed value of $\hbar$, as is usually the case in the articles in which scars are discussed.

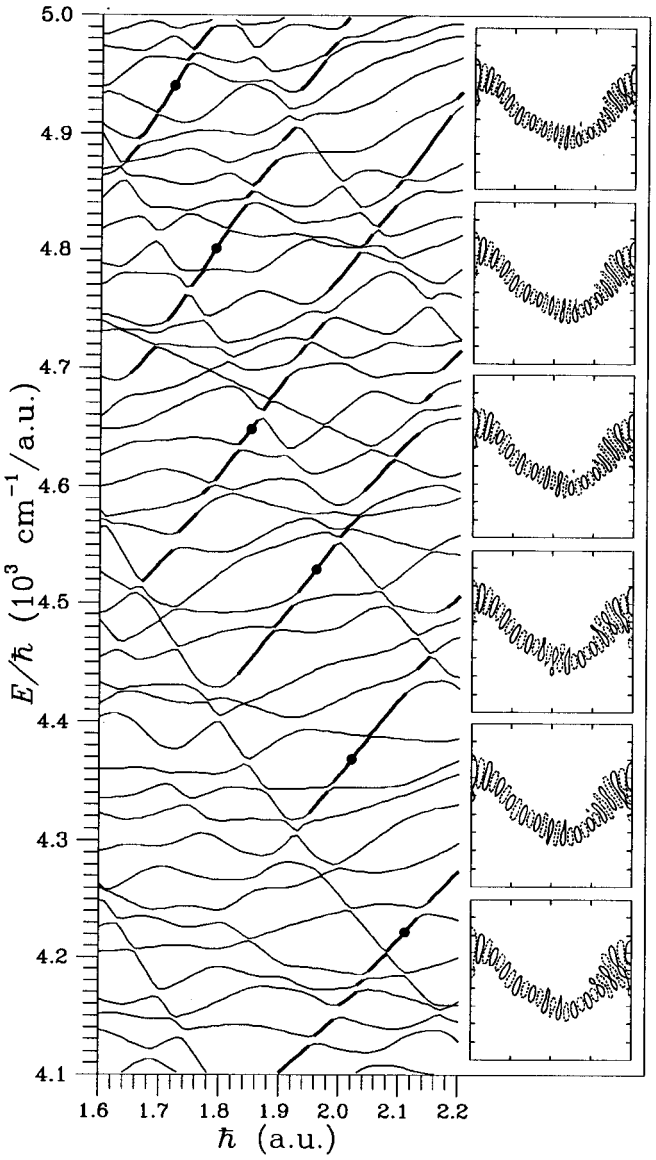

FIG. 11. The region of the correlation diagram showing some rotor states (marked with a thick line). The corresponding diabatic curves exhibit a characteristic positive constant slope. Six scarred wave functions, corresponding to the points marked with dots, are shown in the insets. Two contours corresponding to $\pm 10\%$ of the maximum value of the wave function has been represented in solid and dashed lines, respectively. The axes are the same as in Fig. 1.

Moreover, this last series of ACs constitutes the frontier between a region of regularity, in which the existing ACs are sharp and isolated, and another more chaotic, in which the interactions are more important and the ACs are broader, overlapping and, in general, involve more than two states. In the first region the wave functions present regular nodal patterns, while in the second they correspond to irregular or scarred nodal structures.

At higher values of $\hbar$ the scarred wave functions described above get involved in more complicated interactions, which include in general other states. As a result some states appear scarred by other POs or delocalized between the two isomer wells of the system. One of our conclusions is that these isomerizing states should not be mistaken with true rotor states, appearing at higher values of $\hbar$ or energy, which present a different behavior in the correlation diagram.

ACKNOWLEDGMENT

This work has been supported in part by DGES (Spain) under Contract No. PB95-425.

APPENDIX: CALCULATION OF THE INTERACTION MATRIX ELEMENTS

In this Appendix explicit analytical expressions for the matrix elements $\langle \phi_m | \partial/\partial\hbar | \phi_n \rangle$ between DVR-DGB wave functions are derived.

The vibrational Hamiltonian operator for our system, in the $|R\theta\rangle$ representation, is[43]

$$\langle R\theta|\hat{H}|\Psi\rangle = \langle R\theta|(\hat{T}+\hat{V})|\Psi\rangle = \left[-\frac{\hbar^2}{2\mu_1 R^2}\frac{\partial}{\partial R}\left(R^2\frac{\partial}{\partial R}\right) - \frac{\hbar^2}{2}\left(\frac{1}{\mu_1 R^2}+\frac{1}{\mu_2 r_e^2}\right) \times \frac{1}{\sin\theta}\frac{\partial}{\partial\theta}\left(\sin\theta\frac{\partial}{\partial\theta}\right) + V(R,\theta)\right]\langle R\theta|\Psi\rangle, \quad \text{(A1)}$$

with the following volume element and integration limits:

$$d\tau = R^2 \sin\theta\, dR\, d\theta, \quad 0 \leqslant R < \infty, \quad 0 \leqslant \theta \leqslant \pi. \quad \text{(A2)}$$

Therefore, the Hellmann–Feynman theorem [see Eq. (7)] in this case states that

$$\left\langle \phi_m \left| \frac{\partial}{\partial\hbar} \right| \phi_n \right\rangle = \frac{2}{\hbar(E_n - E_m)}\langle \phi_m|\hat{T}|\phi_n\rangle. \quad \text{(A3)}$$

The DVR-DGB wave functions in the Bačić and Light method are expressed as

$$\langle R\theta|\phi_n\rangle = \left(\frac{2}{\pi}\right)^{1/4} \sum_{j=0}^{j_{\max}} \sum_{\alpha=0}^{j_{\max}} \sum_{i=0}^{m_\alpha - 1} P_j(\cos\theta)\, t_{j\alpha} C_{\alpha i}^{(n)} A_{\alpha i}^{1/4} \times \exp[-A_{\alpha i}(R - R_{\alpha i})^2], \quad \text{(A4)}$$

where all symbols have the same meaning as in Ref. 37; namely, P_j are Legendre polynomials, $t_{j\alpha}$ the DVR transformation matrix elements, $C_{\alpha i}^{(n)}$ the optimized linear coefficients for the nth stationary state, and $A_{\alpha i}$ and $R_{\alpha i}$ the exponents and centers, respectively, of the distributed Gaussian (DGB) functions. The parameters $j_{\max}$ and m_α determine, respectively, the number of DVR points (rays) and the number of Gaussian functions *per* ray. In our calculations, reported in Sec. II A, $j_{\max}+1=45$ DVR points and a basis set of $\Sigma_{\alpha=0}^{j_{\max}} m_\alpha = 416$ Gaussian functions were used.

The matrix elements $\langle \phi_m|\hat{T}|\phi_n\rangle$ for DVR-DGB wave functions result to have the expression

$$\langle \phi_m|\hat{T}|\phi_n\rangle = \hbar^2 (2\pi)^{-1/2}(T_1 + T_2), \quad \text{(A5)}$$

where

$$T_1=\frac{2}{\mu_1}\sum_{j=0}^{j_{\max}}\sum_{\alpha'=0}^{j_{\max}}\sum_{i'=0}^{m_{\alpha'}-1}\sum_{\alpha=0}^{j_{\max}}\sum_{i=0}^{m_{\alpha}-1} t_{j\alpha'}t_{j\alpha}C^{(m)}_{\alpha' i'}C^{(n)}_{\alpha i} \times A^{1/4}_{\alpha' i'}A^{5/4}_{\alpha i}K_{\alpha\alpha' ii'}[-2R_{\alpha i}I_1+(3-2A_{\alpha i}R^2_{\alpha i})I_2 +4A_{\alpha i}R_{\alpha i}I_3-2A_{\alpha i}I_4], \tag{A6}$$

and

$$T_2=\sum_{j=0}^{j_{\max}}\sum_{\alpha'=0}^{j_{\max}}\sum_{i'=0}^{m_{\alpha'}-1}\sum_{\alpha=0}^{j_{\max}}\sum_{i=0}^{m_{\alpha}-1} j(j+1) \times t_{j\alpha'}t_{j\alpha}C^{(m)}_{\alpha' i'}C^{(n)}_{\alpha i}A^{1/4}_{\alpha' i'}A^{1/4}_{\alpha i}K_{\alpha\alpha' ii'}\left[\frac{1}{\mu_1}I_0+\frac{1}{\mu_2 r_e^2}I_2\right]. \tag{A7}$$

In these expressions the following definitions have been used:

$$I_n=\mathscr{T}_n(A_{\alpha\alpha' ii'},R_{\alpha\alpha' ii'}), \tag{A8}$$

$$A_{\alpha\alpha' ii'}=A_{\alpha i}+A_{\alpha' i'}, \tag{A9}$$

$$R_{\alpha\alpha' ii'}=\frac{A_{\alpha i}R_{\alpha i}+A_{\alpha' i'}R_{\alpha' i'}}{A_{\alpha i}+A_{\alpha' i'}}, \tag{A10}$$

and

$$K_{\alpha\alpha' ii'}=\exp\left[-\frac{A_{\alpha i}A_{\alpha' i'}}{A_{\alpha i}+A_{\alpha' i'}}(R_{\alpha i}-R_{\alpha' i'})^2\right], \tag{A11}$$

being

$$\mathscr{T}_n(\gamma,r_0)=\int_0^{\infty}dr r^n e^{-\gamma(r-r_0)^2}. \tag{A12}$$

The integrals $\mathscr{T}_n(\gamma,r_0)$ are easily obtained by means of the recurrence relation

$$\mathscr{T}_{n+2}=r_0\mathscr{T}_{n+1}+\frac{n+1}{2\gamma}\mathscr{T}_n, \tag{A13}$$

knowing that the first two elements are given by

$$\mathscr{T}_0=\left(\frac{\pi}{4\gamma}\right)^{1/2}[1+\mathrm{erf}(r_0\gamma^{1/2})], \tag{A14}$$

and

$$\mathscr{T}_1=\frac{1}{2\gamma}e^{-\gamma r_0^2}+r_0\mathscr{T}_0. \tag{A15}$$

[1] E. E. Nikitin and L. Zülicke, *Theory of Chemical Elementary Processes* (Springer-Verlag, Berlin, 1978); B. H. Bransden and M. R. C. McDowell, *Charge Exchange and the Theory of Ion–Atom Collisions* (Clarendon, Oxford, 1992).

[2] J. V. Neumann and E. Wigner, Z. Phys. **30**, 467 (1929).

[3] See examples in F. Borondo, A. Macías, and A. Riera, Phys. Rev. Lett. **46**, 420 (1981); J. Chem. Phys. **74**, 6126 (1981).

[4] (a) D. W. Noid, M. L. Koszykowski, and R. M. Marcus, Chem. Phys. Lett. **73**, 269 (1980); (b) D. W. Noid, M. L. Koszykowski, M. Tabor, and R. M. Marcus, J. Chem. Phys. **72**, 6169 (1980); (c) R. Ramaswamy and R. A. Marcus, *ibid.* **74**, 1379, 1385 (1981); (d) D. W. Noid, M. L. Koszykowski, and R. M. Marcus, *ibid.* **78**, 4018 (1983); (e) T. Uzer, D. W. Noid, and R. M. Marcus, *ibid.* **79**, 4412 (1983).

[5] M. C. Gutzwiller, *Chaos in Classical and Quantum Mechanics* (Springer, New York, 1990); F. Haake, *Quantum Signatures of Chaos* (Springer-Verlag, Berlin, 1991); L. E. Reichl, *The Transition to Chaos in Conservative Classical Systems: Quantum Manifestations* (Springer-Verlag, New York, 1992); K. Nakamura, *Quantum Chaos: A New Paradigm of Nonlinear Dynamics* (Cambridge University Press, Cambridge, 1993).

[6] M. S. Child, *Semiclassical Mechanics with Molecular Applications* (Clarendon, Oxford, 1991).

[7] M. Joyeux, J. Chem. Phys. **102**, 2816 (1995).

[8] A. M. Ozorio de Almeida, J. Phys. Chem. **88**, 6139 (1984).

[9] F. L. Roberts and C. Jaffé, J. Chem. Phys. **99**, 2495 (1993).

[10] E. J. Heller, J. Phys. Chem. **99**, 2625 (1995).

[11] E. J. Heller, E. B. Stechel, and M. J. Davis, J. Chem. Phys. **73**, 4720 (1980).

[12] K. J. Nordholm and S. A. Rice, J. Chem. Phys. **61**, 203 (1974).

[13] W. A. Lin and L. E. Ballentine, Phys. Rev. Lett. **65**, 2927 (1990); Phys. Rev. A **45**, 3637 (1992).

[14] M. Latka, P. Grigolini, and B. J. West, Phys. Rev. E **50**, 596 (1994); Phys. Rev. A **50**, 1071 (1994); Phys. Rev. E **50**, R3299 (1994).

[15] N. Pomphrey, J. Phys. B **7**, 1909 (1974).

[16] I. C. Percival, J. Phys. B **6**, 559 (1973).

[17] P. Gaspard, S. A. Rice, H. J. Mikeska, and K. Nakamura, Phys. Rev. A **42**, 4015 (1990); T. Takami and H. Hasegawa, Phys. Rev. Lett. **68**, 419 (1992); F. von Oppen, *ibid.* **73**, 798 (1994).

[18] A. A. Stuchebrukhov and R. A. Marcus, J. Chem. Phys. **98**, 6044 (1993); S. A. Schofield, P. G. Wolynes, and R. E. Wyatt, Phys. Rev. Lett. **74**, 3720 (1995).

[19] P. Pechukas, Phys. Rev. Lett. **51**, 943 (1983).

[20] T. Yukawa, Phys. Rev. Lett. **54**, 1883 (1985); X. Yang and J. Burgdörfer, *ibid.* **66**, 982 (1991); S.-J. Wang and S. Y. Chu, Phys. Rev. A **47**, 3546 (1993).

[21] V. I. Arnold, *Mathematical Methods of Classical Mechanics* (Springer-Verlag, New York, 1978).

[22] C. C. Martens, M. J. Davis, and G. S. Ezra, Chem. Phys. Lett. **142**, 519 (1987); J. von Milczewski, G. H. F. Diercksen, and T. Uzer, Phys. Rev. Lett. **76**, 2890 (1996); J. C. Losada, J. M. Estebaranz, R. M. Benito, and F. Borondo, J. Chem. Phys. (to be submitted).

[23] F. J. Arranz, F. Borondo, and R. M. Benito, J. Chem. Phys. **104**, 6401 (1996).

[24] J. Tennyson and S. C. Farantos, Chem. Phys. **93**, 237 (1985); S. C. Farantos and J. Tennyson, J. Chem. Phys. **82**, 800 (1985); Z. Bačić and J. Light, *ibid.* **85**, 4594 (1986); R. M. Benito, F. Borondo, J.-H. Kim, B. G. Sumpter, and G. S. Ezra, Chem. Phys. Lett. **161**, 60 (1989); Z. Bačić, J. Chem. Phys. **95**, 3456 (1991); J. R. Henderson and J. Tennyson, Mol. Phys. **69**, 639 (1990); F. Borondo, A. A. Zembekov, and R. M. Benito, Chem. Phys. Lett. **246**, 421 (1995); J. Chem. Phys. **105**, 5068 (1996); F. J. Arranz, F. Borondo, and R. M. Benito, Phys. Rev. E **54**, 2458 (1996); J. Mol. Struct. Theochem. (in press).

[25] F. Borondo, An. Fis. A **86**, 193 (1990); F. Borondo, J. M. Gomez-Llorente, and R. M. Benito, Laser Chem. **12**, 85 (1992); F. Borondo and R. M. Benito, in *Frontiers of Chemical Physics*, NATO ASI Series C, edited by E. Yurtsever (Kluwer, Dordrecht, 1995); R. M. Benito and F. Borondo, in *Hamiltonian Systems with Three or More Degrees of Freedom*, NATO ASI Series C, edited by C. Simó (Kluwer, Dordrecht, in press).

[26] J. M. Gomez-Llorente, F. Borondo, N. Berenguer, and R. M. Benito, Chem. Phys. Lett. **192**, 430 (1992);

[27] R. Prosmiti, S. C. Farantos, R. Guantes, F. Borondo, and R. M. Benito, J. Chem. Phys. **104**, 2921 (1996).

[28] E. J. Heller, Phys. Rev. Lett. **53**, 1515 (1984); S. W. McDonald and A. N. Kaufmann, *ibid.* **42**, 1189 (1979); Phys. Rev. A **37**, 3067 (1988).

[29] E. G. Bogomolny, Physica D **31**, 169 (1988).

[30] G. G. de Polavieja, F. Borondo, and R. M. Benito, Phys. Rev. Lett. **73**, 1613 (1994).

[31] E. J. Heller, in *Chaos and Quantum Physics*, edited by M. Giannoni, A. Voros, and J. Zinn-Justin (Elsevier, Amsterdam, 1991).

[32] M. J. Davis, Chem. Phys. Lett. **192**, 479 (1992).

[33] T. Takami, Phys. Rev. Lett. **68**, 3371 (1992); Phys. Rev. E **52**, 2434 (1995).

[34] Notice that the expression $\langle\phi_m|\partial/\partial\hbar|\phi_n\rangle$ must not be interpreted as the representation of a quantum operator, but as the scalar product between vectors $\langle\phi_m|$ and $\partial|\phi_n\rangle/\partial\hbar$.

[35] R. Essers, J. Tennyson, and P. E. S. Wormer, Chem. Phys. Lett. **89**, 223 (1982).
[36] R. DeVogelare, in *Contributions to the Theory of Non Linear Oscillations*, edited by S. Lefschetz (Princeton University Press, Princeton, 1958), Vol. IV, p. 53; J. Heagy and J. M. Yuan, Phys. Rev. A, **41**, 571 (1990); C. Jung and P. H. Richter, J. Phys. A, **23**, 2847(1990).
[37] Z. Bačić and J. Light, Annu. Rev. Phys. Chem. **40**, 469 (1989).
[38] F. T. Smith, Phys. Rev. **179**, 111 (1969).
[39] A. Macías and A. Riera, Phys. Rep. **90**, 300 (1982).
[40] R. P. Feynman and T. A. Welton, Phys. Rev. **56**, 340 (1939).
[41] Although the range spanned by the angular variable θ goes from 0 to π we use for the regular states the notation corresponding to a harmonic description, in which the quantum bending number corresponds to double the number of nodes in θ. This quantum number can only be even due to the fact that we are considering states with total angular momentum equal to zero. See the discussion in I. N. Levine, *Molecular Spectroscopy* (Wiley, New York, 1975), p. 271.
[42] W. H. Miller, J. Chem. Phys. **72**, 99 (1980).
[43] J. Tennyson and B. T. Sutcliffe, J. Chem. Phys. **77**, 4061 (1982).